Engineering Solid Mechanics12 (2024) 353-362

Contents lists available at GrowingScience

Engineering Solid Mechanics

homepage: www.GrowingScience.com/esm

Analysis of the effects of vickers indentation-induced defects on the strength and probability of failure of float glass during biaxial flexure testing

Walid Dairi[a*] and Mohamed Hamidouche[a]

[a]*Emerging Materials Research Unit Institution: Institute of Optics and Precision Mechanics, Ferhat ABBAS University of Setif1, Setif 19000, Algeria*

ARTICLEINFO

Article history:
Received 22 January 2023
Accepted 5 June 2024
Available online
5 June 2024

Keywords:
Float glass
Vickers indentation
Biaxial flexure
Weibull distribution

ABSTRACT

This study examines the impact of indentations on the strength of float glass. Using the Vickers indentation method with loads of 1N and 10N, we created defects at varying distances from the point of contact. Biaxial flexure tests revealed that indentations with 1N at 18mm decreased the strength, while those with 10N and shorter distances from the point of contact increased the strength. Weibull distribution analyses showed a correlation between the load, distance, and the Weibull modulus, highlighting the influence of defect size on the probability of rupture.

1. Introduction

The study aims to examine the samples' resistance to biaxial flexure by analyzing flaws resulting from Vickers indentation at varying distances from the contact point. The study seeks to comprehend the response of the samples to failure or deformation when subjected to specified loads. In addition, the study aims to examine the distribution of flaws by utilizing the Weibull distribution to mathematically represent the likelihood of sample failure or rupture based on the distance from the contact point and the applied stress. The sensitivity to the load is assessed by examining the variations in the values of eta and beta as the load increases. This facilitates a more comprehensive comprehension of how flaws or damage alter under varying limitations. The study's objective is to gather data that can be used to enhance materials by identifying their areas of vulnerability or resilience. This analysis is essential for guiding material optimization in order to improve their resistance to biaxial flexure.

Glass is a fragile substance that is not made of metal and has the property of linear elasticity (Lewandowski et al., 2005). Soda-lime glass is extensively utilized in the manufacturing of windows, containers, and various other glass products. Additionally, it is a crucial material for multiple glass research projects (Zarzycki, 1977). Glass exhibits the characteristics of a highly elastic solid, adhering to Hooke's law, and does not display any noticeable plastic deformation prior to breaking. A fracture occurs abruptly, without any preceding indications, once the final tensile stress surpasses its limit. This behaviour is characteristic of materials that are prone to breaking easily (Li et al., 2013). The float glass method is commonly employed for the production of flat glass on a global scale. During the creation of float glass, tin diffuses from the bath. The process involves pouring molten glass into a liquid tin bath, where it undergoes cooling and solidification, resulting in the formation of two flat sides of a glass sheet. The portion of the surface that is in touch with the tin bath is referred to as the "tin side," whilst the top surface is known as the “air side”. The surfaces of float glass may display varying qualities as a result of disparities in composition and structure (Townsend et al., 1998).

The existence of minor imperfections has a significant impact on the resistance of brittle materials, such as glass and ceramics. These imperfections, commonly known as microcracks, are considered unavoidable and widespread in these materials (Lawn et al., 1983). The strength of glass is influenced by both its inherent qualities as a bulk material and the

* Corresponding author.
E-mail addresses: Walid_opt04@yahoo.fr (W. Dairi)

ISSN 2291-8752 (Online) - ISSN 2291-8744 (Print)

doi: 10.5267/j.esm.2024.6.001

surrounding environment it is subjected to. The fundamental characteristics of glass, such as its hardness and modulus of elasticity, are mainly influenced by factors such as the strength of the bonds between atoms, the connectedness of atomic networks, the density of the material, and its thermal history. Furthermore, deviations in the composition of glass might also have an impact on its overall qualities (Rodrigues et al., 2022).. The presence of defects in glass can have a significant impact on its properties and applications. The defects in glass products can arise from various sources, such as structural faults, point defects affecting diffusion, color, and composition, as well as helical defects influencing crystal growth (Matusova & Hruskova, 2022). Identifying and characterizing these defects are critical to ensure the quality and reliability of glass materials. Techniques such as pulsed thermography have been employed to detect defects in archaeological glass, so providing an insight into the preservation status of historical artifacts (Ciarella et al., 2023). In addition, advancements in machine learning have facilitated the efficient exploration of the energy landscape of glass models to identify specific classes of defects, such as rare two-level systems with quantum tunneling effects, thereby providing insights into their microscopic nature (Marcos, 2022). La résistance du verre flotté avec des défauts peut être mesurée en utilisant diverses méthodes. The fracture resistance of basic float glass is influenced by its physicochemical properties and surface defects formed during manufacture and handling, which have an impact on its structural strength (Symoens et al., 2023). Detecting defects in float glass is critical for quality control, using methods such as annular defect detection for surface edge defects (Rodichev & Veer, 2010). Pisano, G shown in his work that the lower limit of glass strength is due to production controls, and that the statistical distribution of crack size influences the macroscopic strength of glass (Pisano, 2017). Symoens et al. have demonstrated that Weibull and normal distributions are suitable for many defects subjected to a load (Symoens et al., 2023). Madjoubi, M. A. et al shown that the presence of erosion-induced defects in glass significantly affects its strength. After 1 hour of erosion, these defects become predominant in determining the strength of the glass (Madjoubi et al., 1999). The work of Wakabayashi, C. et al. has demonstrated the significance of Weibull parameters, estimated from the original distribution of defect sizes, as well as their relationships. This approach becomes valuable in the analysis of the reliability of fragile materials (Wakabayashi et al., 2009). Hardness is a measure of a material's resistance to permanent deformation or indentation by a harder object. In the case of glass, its hardness is generally high due to the strong bond strength between its constituent atoms(Tao & Wang, 2021). This means that glass is less likely to deform or undergo permanent deformation under the application of external forces. However, it is important to note that even though glass is considered a hard material, it is not completely deformable and can break or crack when subjected to significant stresses(Januchta et Smedskjaer, 2019).

Elasticity, on the other hand, is a measure of glass's ability to deform reversibly under the application of external forces. The modulus of elasticity of glass is a measure of its stiffness, i.e., its resistance to elastic deformation(Bauchy, 2019). Glass typically has a high modulus of elasticity, indicating that it tends to retain its shape and recover its initial form after being subjected to elastic stresses. However, it is crucial to note that glass is a brittle material, meaning it can break rather than undergo plastic deformation when subjected to significant stresses(Surdyka et al., 2014).
This study makes a significant contribution in several key areas. Firstly, it sheds light on the resistance of float glass samples to biaxial bending, providing a thorough understanding of rupture and deformation mechanisms under specific loads. By examining defects generated by Vickers indentation at different distances from the point of contact, it allows for the precise mapping of areas sensitive to failure or rupture.

Furthermore, the use of the Weibull distribution to analyse the distribution of defects provides a probabilistic model to assess the probability of failure of samples based on the distance from the point of contact and the applied load. This offers crucial information for predicting material behaviour under variable loading conditions.
Moreover, the study helps understand load sensitivity by observing variations in eta and beta values, aiding in apprehending the transformation of defects or damages in response to different stresses. This knowledge is essential for designing more resilient materials and guiding their optimization by identifying areas of fragility or strength.

2. Weibull analysis

The foundation of all statistical models for material failure is the premise that flaws, which raise local stresses and ultimately cause premature failure, are responsible for discrepancies between ideal and real performances (Tiryakioğlu, 2015). The distribution of flaws can be associated with statistical distributions of mechanical parameters related to rupture, such as fatigue life, rupture toughness, elongation, and rupture stress (Barbosa et al., 2019). According to statistics, the "weakest link" is the worst (biggest) fault, which defines the mechanical qualities associated with rupture. The "weakest link" notion is applicable in circumstances similar to a chain breaking when one of its links gives way. Wallodi Weibull presented an empirical distribution for ceramics and metals based on the principle of the "weakest link," which has subsequently gained widespread use (Tiryakioğlu & Campbell, 2010). According to T. Li et al. (2017), the Weibull distribution's cumulative probability function is expressed as follows.

$$P = 1 - \exp\left[-\left(\frac{\sigma - \sigma_T}{\sigma_0} \right)^m \right] \tag{1}$$

where P represents the failure probability at a stress (strain, fatigue life, etc.) of r or less. The value below which no sample is likely to fail is known as the threshold value, or σ_T. The shape parameter, or Weibull modulus, is denoted by the letter m, while the scale parameter is denoted by the term σ_0.

The Weibull probability plot is one of the most widely used techniques for displaying Weibull fits to data. Eq. (1) can be rewritten as follows after rearrangement (Pardini & Manhani, 2002).

$$\ln\left[-\ln\left(1-P\right)\right] = m\ln\left(\sigma-\sigma_T\right) - m\ln\left(\sigma_0\right). \tag{2}$$

When the left side of Eq. (2) is plotted against ln (σ - σT), it can be shown that the equation has a linear form with a y-intercept of $-m\ln(\sigma 0)$ and a slope of m. An alternative way to plot the left side of the equation against ln(σ) is to generate the Weibull probability plot. A linear relationship is only produced by this presenting approach when $\sigma T = 0$. The width or extent of the distribution of defect sizes is described by the Weibull modulus m, a material property that describes the dispersion of defects. Defects with varying sizes are found in a population when m is high. The formula for the probability *Ps* is (Trustrum & Jayatilaka, 1979).

$$P_s = 1 - P \tag{3}$$

In order to accomplish this, all measured values must be arranged in ascending order, and then each value of σi must be assigned a failure probability, represented by Pi. The values of the variable i range from 1 to *N*, where *N* is the total number of measurements in the sample under test. One of the primary probability estimators that is frequently used is used for this (Zerbo et al., 2019).

$$P_i = \frac{i}{\left(N+1\right)} \tag{4}$$

N is the number of measured values.

3. Mechanical characterization

3.1 Materials and Methodology

Utilized glass

The glass material utilized in our experiment is procured from Mediterranean Float Glass (MFG spa). Mediterranean Float Glass (MFG SPA) is a well-known African maker of flat glass. It was established in 2007 and is a branch of CEVITAL.It stands out due to the 3 mm thickness of the float glass that is produced locally. Table 1 provides a comprehensive and detailed overview of all the qualities and specifications of this material.

Table 1. Properties of the glass used

Proprieties	Values	Proprieties	Values
Modulus of elasticity	72 GPa	Transition temperature	502.8 °C
Poisson's ratio	0.22	Density	2.51 g/cm3
Vickers hardness	4.7 GPa	Optical transmission	92%
Toughness	0.74 MPa$\sqrt{m}$	Refractive index	1.511
Thermal expansion coefficient	8.1 × 10-6°C-1		

The chemical composition data is acquired using The X-ray fluorescence technique (XRF) and is presented in **Table 2.**

Table 2. Chemical composition of the glass used

The oxides	mass%	The oxides	mass%
SiO_2	70.1	AL_2O_3	0.826
Na_2O	14.4	K_2O	0.515
CaO	9.12	SO_3	0.156
MgO	4.79	Fe_2O_3	0.0749

3.2 Flexural strength

The QATM micro durometer for Vickers, Knoop, and Brinell tests loads ranging from 0.25 g to 62.5 kg. All durometers have user-friendly software for easy operation, analysis, and documentation of data. Turrets with 6 or 8 diamonds or alternative test lenses can be mounted, making the Vickers, Knoop, and Brinell hardness tests very easy to pass. The microscope utilized is a Euromex universal microscope of the type OXION, with an 8 MP camera attached to a computer, allowing the observations to be visualized on a screen. The results are processed using an alpha version of Image Focus software. The magnification ranges from 50 to 1,000 times.

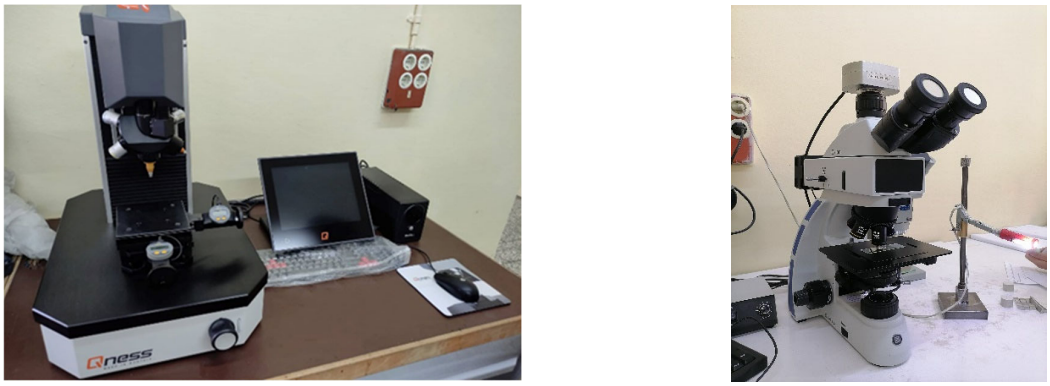

Fig. 1. instrument of indentation model “QNESS Q30 M”and visualisation “Euromex universal microscope of the type OXION”

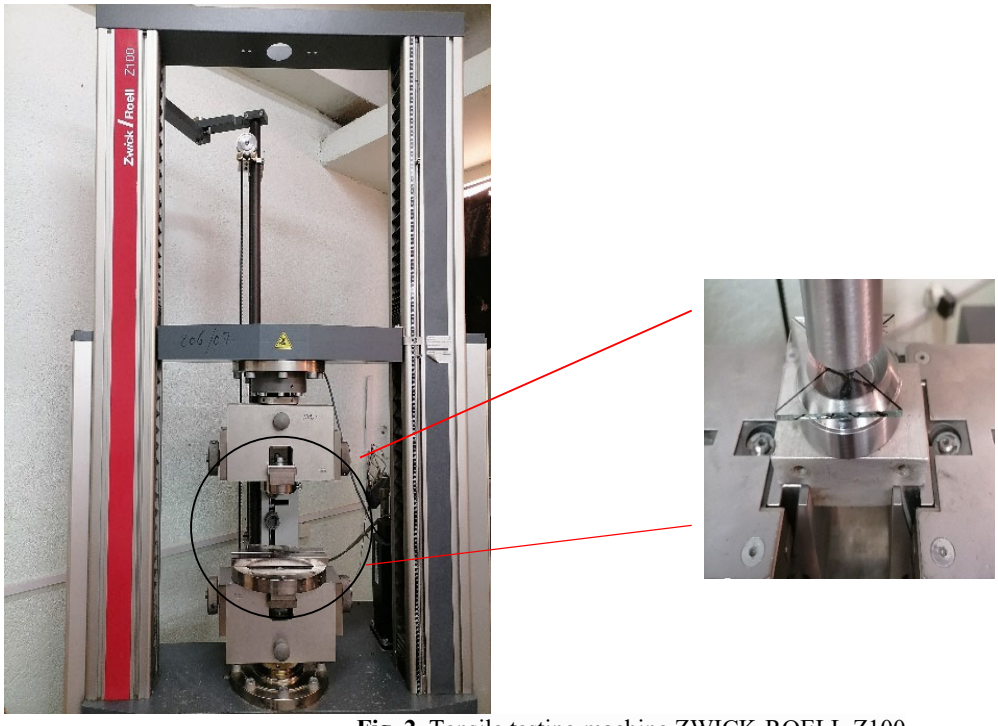

Fig. 2. Tensile testing machine ZWICK-ROELL Z100

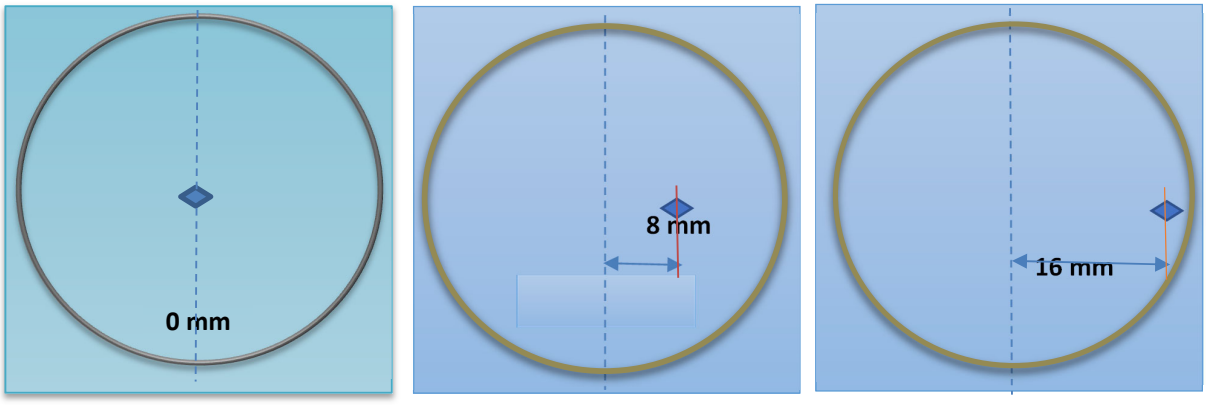

Fig. 3. Different positions of the impressions in relation to the ring boundary

Intentional defects were introduced on the underside of the samples, as shown in **Fig. 4b**. The load rate was maintained at 0.3 mm/min throughout the tests. Two different loads, 1 N and 10 N, were applied to a sample for 15 seconds each one. These tests involved varying the distance from the centre of the sample, ranging from 8 mm to 16 mm from the centre, as shown in **Fig. 3**. The samples used in these tests had dimensions of 50×50 mm². Concentric biaxial bending tests, as depicted in **Fig. 4a**, offer a notable advantage compared to three- and four-point bending devices by successfully reducing the impact of edge flaws. This enables the assessment of inherent or innate strength. For these experiments, sets of 15 samples were utilized, all having the same size of 50×50 mm². The testing apparatus consists of two rings, an inner ring with a diameter of 16 mm and an outer ring with a diameter of 36 mm. The fracture stresses (σ) were calculated using the appropriate relation. The precise methodology of these calculations is essential for accurately determining the material's strength characteristics.

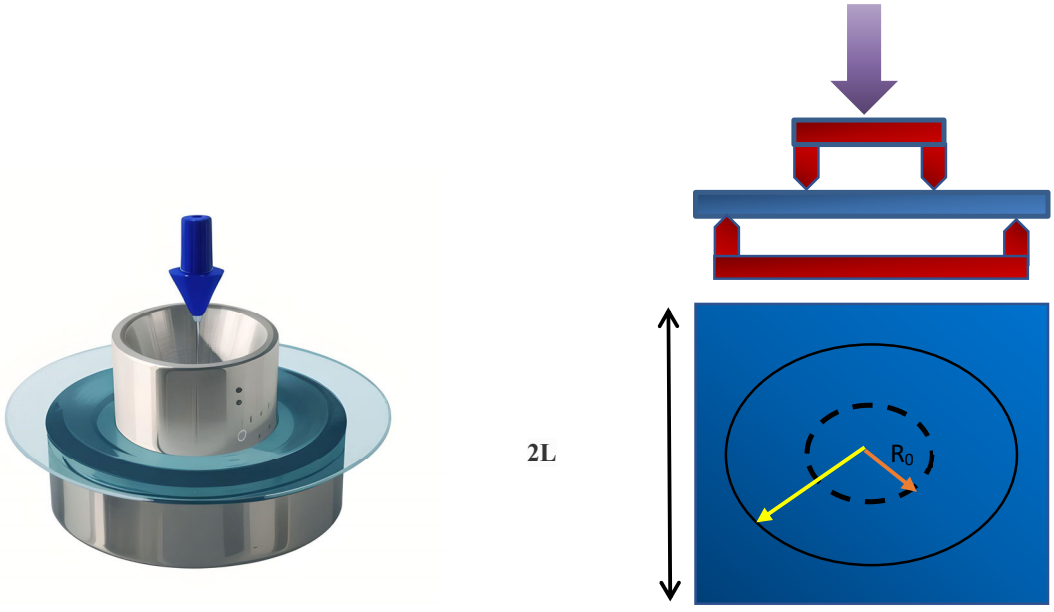

Fig. 4. Concentric biaxial flexural tests

Fig. 4a depicts the strength characterization utilizing concentric biaxial flexural tests. This approach has a substantial benefit over three- and four-point bending devices because it efficiently eliminates edge flaws, allowing for the assessment of intrinsic strength. In these studies, 15 samples with equal dimensions of 50 × 50 mm² were employed. The apparatus used in this investigation includes inner and outer rings with diameters of 16 mm and 36 mm, respectively. **Fig. 4b** depicts defects that were purposefully introduced on the underside of the samples. The loading rate was kept constant at 0.3 mm/min throughout all testing. The rupture stresses (σ) were computed according to the suitable relationship. Furthermore, the study included a variation in the distance between. The rupture stresses (σ) were evaluated based on the relationship (Faci, 2018):

$$\sigma = \frac{3F_R}{2\pi h^2}\left[(1+\nu)\ln\frac{R_1}{R_2} + (1+\nu)\left(R_1^2 - R_0^2\right)/2R_2^2\right] \tag{5}$$

In this equation, we use the following variables: F_R represents the fracture force, ν is the Poisson's ratio of glass, established at 0.22. The value of h corresponds to the thickness of the sample was positioned at a thickness of 3 mm. Concerning the ring radii, R0 represents the measurement of the inner ring's radius, which is 8 mm, while R1 corresponds to the evaluation of the outer ring's radius, which is 18 mm.

$$R_2 = L\left(1+\sqrt{2}\right)/2 \approx 1.21L \tag{6}$$

Measuring the length of the square sample side gives 50 mm, which corresponds to a value of 2L.

4. Results and discussions

Values of eta (η) and beta (β) for the loads of 1 N and 10 N, as well as for the different distances (0 mm, 8 mm, and 16 mm), are grouped in **Table 3** and **Table 4**, respectively.

Table 3. Values of eta (η) and beta (β) for P = 1N

	18mm	10mm	2mm
eta" (η)	75,292	98,022	109,61
beta" (β)	6	3	2

Table 4. Values of eta (η) and beta (β) for P = 10N

	18mm	10mm	2mm
eta" (η)	41,653	51,466	105,59
beta" (β)	14	5	6

When a 1 N load is applied, the values of eta vary significantly based on the distance between the centre and the point of contact of the sample. For instance, at a distance of 0 mm from the centre and 18 mm from the point of contact, eta reaches 75.292. This value decreases at 8 mm from the centre and 10 mm from the point of contact (98.022), then increases at 16 mm from the centre and 2 mm from the point of contact (109.61).

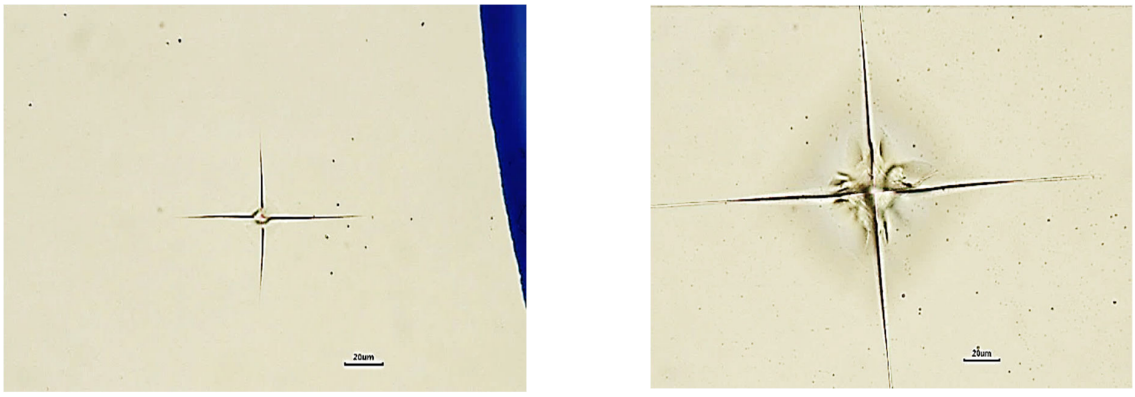

(a) (b)

Fig. 5. Microscopy of indented glass: (a) imprint caused by P = 1N, (b) imprint caused by P = 10N

The examination of **Fig. 5** centres on the indentation imprints found on a glass plate under two distinct loads: P = 1N and P = 10N. Microscopic investigations indicate notable disparities in the attributes of the imprints, specifically regarding the extent of the radial fissures between imprints (a) and (b). Moreover, the area of the impression created by a force of P = 10N is considerably greater than the area produced by P = 1N. The existence of residual stresses, possibly caused by the indentation, is indicated by the presence of a highlighted area surrounding the impression of P = 10N.

These findings highlight that the escalation in applied force, from 1N to 10N, resulting in a substantial augmentation in structural deterioration of the glass material. The heightened radial fissures and larger impression provide as clear evidence of the escalated generated stresses. Furthermore, the existence of residual strains surrounding the impression of P = 10N indicates that the energy exerted during indentation resulted in permanent deformation of the material.

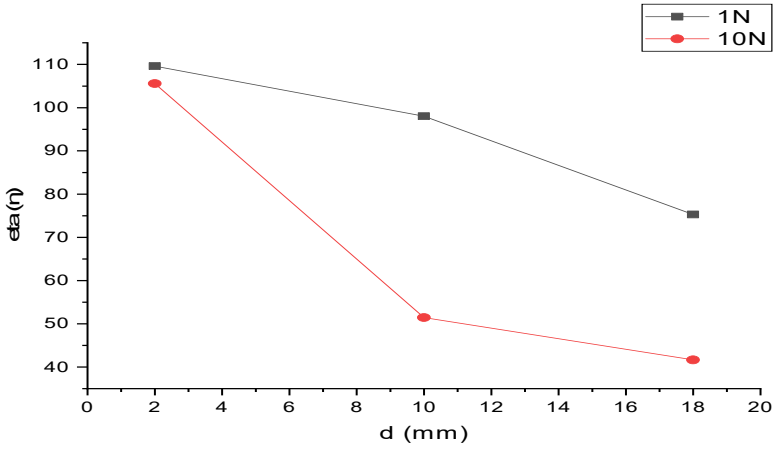

Fig. 6. Evolution of eta (η) as a function of the load and the distance relative to the ring

When the load increases to 10N, the values of eta also show a proportional increase with the distance. For instance, at 0mm from the centre, eta stands at 41.653, then at 8mm from the centre, it climbs to 51.466, reaching a notable value of 105.59 at 16mm from the centre. The results of eta for the 1N and 10N loads, as presented in **Fig. 6**, reveal a trend where eta increases as the indentation defect gets closer to the ring's point of contact. Furthermore, the eta values for the 10N load are lower than those for the 1N load. These differences could result from the complex interaction between the stresses induced by the indentation and those generated by the ring's contact. As the indentation defect approaches the point of contact, the stresses induced by the indentation can interact with the existing stresses caused by the ring's contact. These interactions could alter the distribution and transmission efficiency of stresses within the material. It is possible that the response to a 10N load is more sensitive to interactions, which could explain the observed decrease in eta values compared to a 1N load. Variations in how these stresses interact at different depths of indentation and contact with the ring could influence force transmission and thus have an impact on eta values. **Fig. 7** presents data on beta values for 1N and 10N loads as a function of distance from the center and the ring's point of contact. Observations indicate a similar overall trend for both loads: beta values increase as the Vickers indentation defect moves away from the ring's point of contact. Beta values for defects created with a 10N load are higher than those obtained with a 1N load.

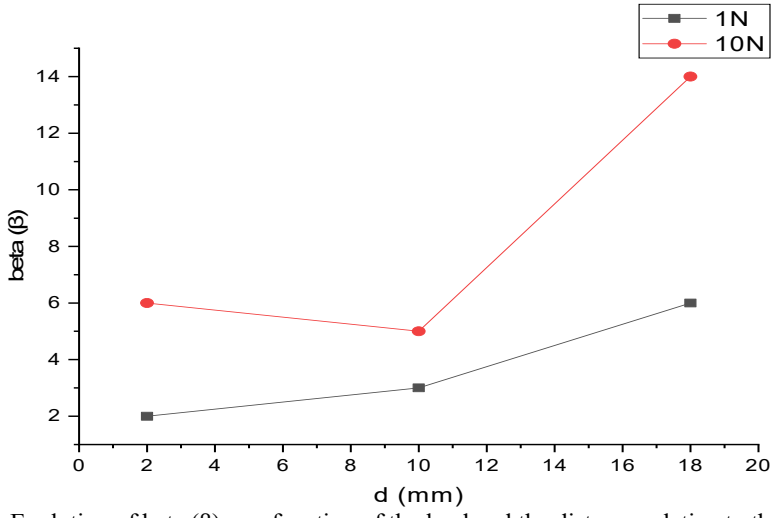

Fig. 7. Evolution of beta (β) as a function of the load and the distance relative to the ring

For a 1N force, beta values increase significantly, reaching 6 when positioned at 0 mm from the centre and 18 mm from the point of contact. Then, they gradually decrease to reach 3 at 8 mm from the centre and 10 mm from the point of contact before decreasing further to 2 at 16 mm from the centre and 2 mm from the point of contact. For a 10N load, beta values follow a similar trend. They are higher, reaching 14 at 0 mm from the centre, then decrease to 5 at 8 mm from the centre. Then, these values slightly increase to reach 6 at 16 mm from the centre. These results highlight a notable variation in material strength based on both the applied load and the distance from the centre and the sample's point of contact. The observed changes in beta values suggest alterations in the distribution of material strength levels, indicating a different sensitivity to loads and positions. These observations could indicate the existence of distinct stress zones within the sample related to the load position, thus influencing material strength. Variations in beta could also reflect irregularities within the material itself or different rupture mechanisms depending on the load's location. The Weibull curves presenting experimental data for 1N and 10N loads at different distances are grouped in **Fig. 8**. Unimodal distributions are observed, indicating the existence of a single population of rupture stresses, as suggested by Weibull's unimodal graph. By varying the distances of Vickers indentation defects with 1N and 10N loads relative to the ring's point of contact in a biaxial flexure test, the Weibull modulus was determined. Results reveal that for a defect created with a 1N load and located at 18mm from the point of contact, the modulus is 6, while for the same distance with a 10N load, the modulus is 15. At a distance of 10mm from the point of contact, the modulus is 2 for a 1N load and 4 for a 10N load. Finally, at a distance of 2mm from the point of contact, the modulus is 2 for a 1N load and 6 for a 10N load. Initially, at a distance of 18mm from the contact point, the Weibull modulus is 6 with a load of 1N and 15 with a load of 10N. This observation suggests that at this very far distance from the contact site, increasing the indentation load leads to a significant increase in defect homogeneity, as evidenced by a higher value of the Weibull modulus. It appears that the residual constraints induced by the ring play a decisive role in the creation and distribution of indentation defects, and that higher loads promote a more uniform distribution of defects.

Subsequently, at a distance of 10mm from the point of contact, the Weibull modulus is 2 with a load of 1N and 4 with a load of 10N. This observation highlights that even at an intermediate distance, the indentation load continues to significantly influence the homogeneity of defects, albeit to a lesser extent than at the 18mm distance. Therefore, it appears that the residual constraints induced by the ring have a less pronounced effect at this distance, but nonetheless remain a key factor in the creation of defects.

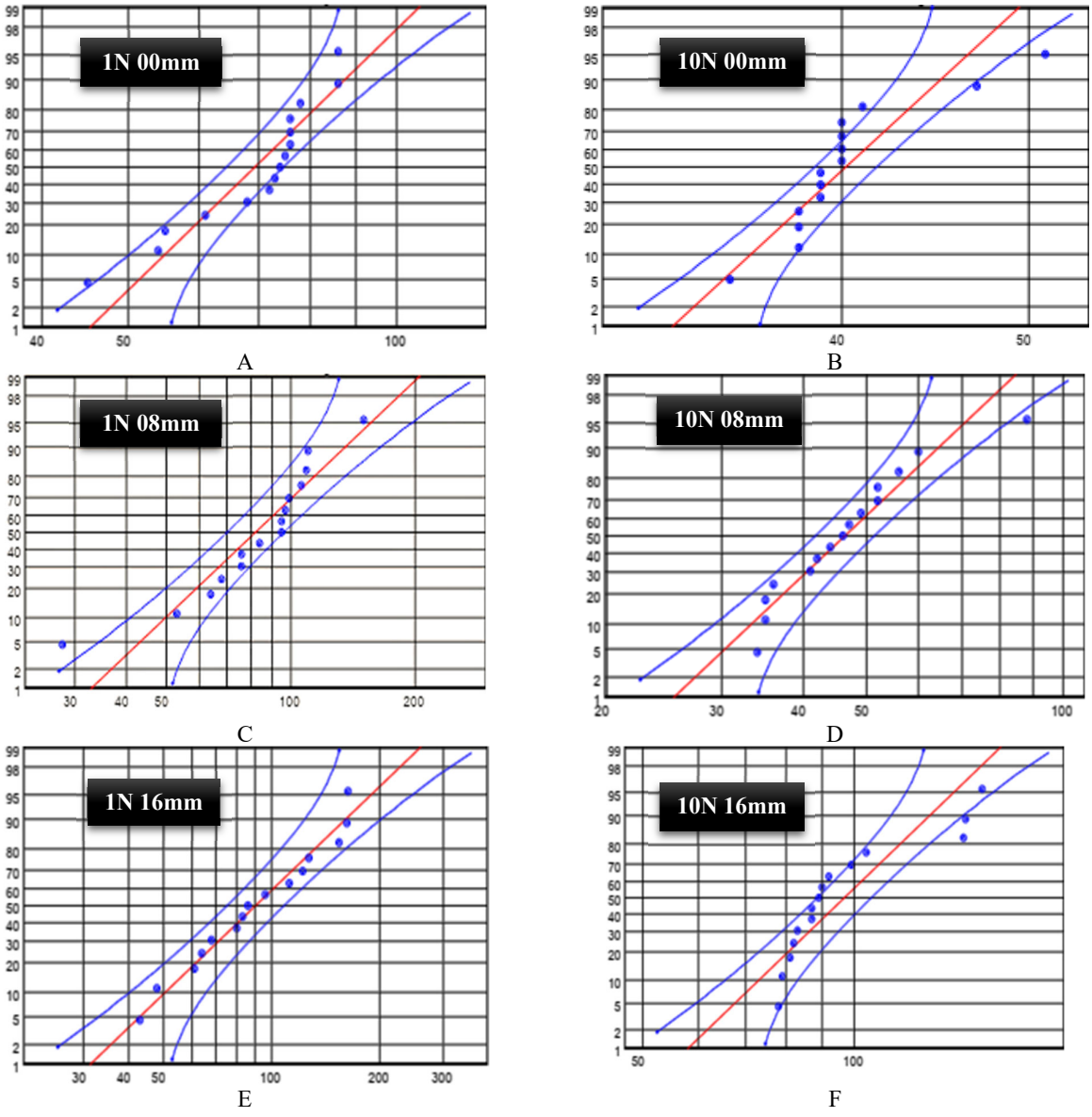

Fig. 8. Graphs of Weibull (A, B, C, D, E, F) for Three Distances (0mm, 8mm, 16mm) and Two Loads (1N and 10N)

At a distance of 2mm from the contact point, the Weibull modulus is 2 with a load of 1N and 6 with a load of 10N. This extreme proximity of the contact site results in a maximum concentration of stresses, which amplifies the variability of indentation defects. It appears that the residual constraints induced by the ring play a particularly influential role at this very close distance, and higher loads can amplify this influence by promoting a more uniform distribution of defects.

5. Conclusion

In conclusion, the observations of the beta and eta values for the Weibull distribution as a function of distance from the centre and the contact point indicate interesting trends. At 0 mm from the centre and 18mm from the contact point, the beta values are higher, suggesting a more stretched or elongated distribution. However, these values gradually decrease at 3 to 8 mm from the centre and 10 mm from the contact point, then slightly increase at 2 to 16 mm from the centre and 2 mm from the contact point. As the load increases to 10 N, the eta values also increase with distance. This increase may be linked to a different material response to higher loads, with a significant increase observed at greater distances from the centre. Regarding the beta values for a 10 N load, they exhibit a complex trend. The values are higher at 0mm from the centre, decrease at 5 to 8 mm from the centre, then slightly increase at 6 to 16mm from the centre. This suggests a nonlinear variation of the Weibull distribution based on distance and load. The results obtained in this study on determining the Weibull coefficient by varying the distances of defects created by Vickers indentation with loads of 1N and 10N during a biaxial flexural test demonstrate a significant correlation between the applied load, the distance from the contact point, and the Weibull coefficient.

It is clear that increasing the applied load leads to a notable increase in the Weibull coefficient, highlighting a direct relationship between defect size and the probability of material failure. This trend is more pronounced when defects are located at shorter distances from the ring's contact point.

References

Barbosa, J. F., Correia, J. A. F. O., Freire Júnior, R. C. S., Zhu, S. P., & De Jesus, A. M. P. (2019). Probabilistic S-N fields based on statistical distributions applied to metallic and composite materials: State of the art. *Advances in Mechanical Engineering*, *11*(8), 1–22. https://doi.org/10.1177/1687814019870395

Bauchy, M. (2019). Topological Constraint Theory and Rigidity of Glasses. *21st Century Nanoscience – A Handbook*, *May*, 13-1-13–20. https://doi.org/10.1201/9780367333003-13

Ciarella, S., Khomenko, D., Berthier, L., Mocanu, F. C., Reichman, D. R., Scalliet, C., & Zamponi, F. (2023). Finding defects in glasses through machine learning. *Nature Communications*, *14*(1), 4229. https://doi.org/10.1038/s41467-023-39948-7

Faci, A. (2018). *No TitleInfluence des paramètres d'érosion sur la résistance mécanique d'un verre sablé : analyse statistique*. 'Université Ferhat ABBAS - Sétif 1.

Januchta, K., & Smedskjaer, M. M. (2019). Indentation deformation in oxide glasses: Quantification, structural changes, and relation to cracking. *Journal of Non-Crystalline Solids: X*, *1*(December 2018), 100007. https://doi.org/10.1016/j.nocx.2018.100007

Lawn, B. R., Dabbs, T. P., & Fairbanks, C. J. (1983). Kinetics of shear-activated indentation crack initiation in soda-lime glass. *Journal of Materials Science*, *18*(9), 2785–2797. https://doi.org/10.1007/BF00547596

Lewandowski, J. J., Wang, W. H., & Greer, A. L. (2005). Intrinsic plasticity or brittleness of metallic glasses. *Philosophical Magazine Letters*, *85*(2), 77–87. https://doi.org/10.1080/09500830500080474

Li, T., Griffiths, W. D., & Chen, J. (2017). Weibull Modulus Estimated by the Non-linear Least Squares Method: A Solution to Deviation Occurring in Traditional Weibull Estimation. *Metallurgical and Materials Transactions A: Physical Metallurgy and Materials Science*, *48*(11), 5516–5528. https://doi.org/10.1007/s11661-017-4294-4

Li, X. Y., Jiang, L. B., Zhang, X. W., Zhang, X., & Yan, Y. (2013). The influence of different surface compressive stress on the wettability of ion-exchanged float aluminosilicate glass. *Advanced Materials Research*, *704*, 105–109. https://doi.org/10.4028/www.scientific.net/AMR.704.105

Madjoubi, M. A., Bousbaa, C., Hamidouche, M., & Bouaouadja, N. (1999). Weibull statistical analysis of the mechanical strength of a glass eroded by sand blasting. *Journal of the European Ceramic Society*, *19*(16), 2957–2962. https://doi.org/https://doi.org/10.1016/S0955-2219(99)00087-4

Marcos, C. (2022). *Crystallography Introduction to the Study of Minerals* (pp. 193–233). springer.

Matusova, M., & Hruskova, E. (2022). Analysis of defects of glass products. *IOP Conference Series: Materials Science and Engineering*, *1256*(1), 012016. https://doi.org/10.1088/1757-899x/1256/1/012016

Pardini, L. C., & Manhani, L. G. B. (2002). Influence of the Testing Gage Length on the Strength, Young's Modulus and Weibull Modulus of Carbon Fibres and Glass Fibres. *Materials Research*, *5*(4), 411–420. https://doi.org/10.1590/s1516-14392002000400004

Pisano, G. (2017). *The statistical characterization of glass strength: From the micro- to the macro-mechanical response*. 205.

Rodichev, Y., & Veer, F. (2010). Fracture resistance, surface defects and structural strength of glass. *Challenging Glass 2 - Conference on Architectural and Structural Applications of Glass, CGC 2010*, *May*, 363–373.

Rodrigues, B. P., To, T., Smedskjaer, M. M., & Wondraczek, L. (2022). Mechanical Properties of Oxide Glasses. *Reviews in Mineralogy and Geochemistry*, *87*(1), 229–281. https://doi.org/10.2138/rmg.2022.87.06

Surdyka, N. D., Pantano, C. G., & Kim, S. H. (2014). Environmental effects on initiation and propagation of surface defects on silicate glasses: Scratch and fracture toughness study. *Applied Physics A: Materials Science and Processing*, *116*(2), 519–528. https://doi.org/10.1007/s00339-014-8552-7

Symoens, E., Van Coile, R., Jovanović, B., & Belis, J. (2023). Probability Density Function Models for Float Glass under Mechanical Loading with Varying Parameters. In *Materials* (Vol. 16, Issue 5). https://doi.org/10.3390/ma16052067

Tao, Y., & Wang, X. (2021). Revealing the atomic-scale origin of simultaneously enhanced hardness and crack resistance in a single phase material. *Journal of Applied Physics*, *129*(15). https://doi.org/10.1063/5.0046733

Tiryakioğlu, M. (2015). Weibull Analysis of Mechanical Data for Castings II: Weibull Mixtures and Their Interpretation. *Metallurgical and Materials Transactions A: Physical Metallurgy and Materials Science*, *46*(1), 270–280. https://doi.org/10.1007/s11661-014-2610-9

Tiryakioğlu, M., & Campbell, J. (2010). Weibull analysis of mechanical data for castings: A guide to the interpretation of probability plots. *Metallurgical and Materials Transactions A: Physical Metallurgy and Materials Science*, *41*(12), 3121–3129. https://doi.org/10.1007/s11661-010-0364-6

Townsend, P. D., Can, N., Chandler, P. J., Farmery, B. W., Lopez-Heredero, R., Peto, A., Salvin, L., Underdown, D., & Yang, B. (1998). Comparisons of tin depth profile analyses in float glass. *Journal of Non-Crystalline Solids*, *223*(1–2), 73–85. https://doi.org/10.1016/S0022-3093(97)00348-7

Trustrum, K., & Jayatilaka, A. D. S. (1979). On estimating the Weibull modulus for a brittle material. *Journal of Materials Science*, *14*(5), 1080–1084. https://doi.org/10.1007/BF00561290

Wakabayashi, C., Yasuda, K., & Shiota, T. (2009). Estimation of Weibull parameters from parameters of initial distribution of flaw size. *Journal of Physics: Conference Series*, *191*, 2–7. https://doi.org/10.1088/1742-6596/191/1/012006

Zarzycki, J. (1977). Propriétés mécaniques des verres. *Revue de Physique Appliquée*, *12*(5), 789–796. https://doi.org/10.1051/rphysap:01977001205078900

Zerbo, L., Seynou, M., Sorgho, B., Lecomte-Nana, G., Gomina, M., & Blanchart, P. (2019). Microstructure and Weibull distribution of rupture strength of clay-talc ceramics. *Ceramica*, *65*(374), 240–245. https://doi.org/10.1590/0366-69132019653742518